Separate Absorption and Modulation Mach-Zehnder Wavelength Converter

Anna Tauke-Pedretti, *Student Member, IEEE,* Matthew M. Dummer, *Student Member, IEEE,*
Matthew N. Sysak, *Member, IEEE,* Jonathon S. Barton, *Member, IEEE,* Jonathan Klamkin, *Student Member, IEEE,*
James W. Raring, *Member, IEEE,* and Larry A. Coldren, *Fellow, IEEE.*

Abstract— A monolithic separate absorption and moduation region (SAM) wavelength converter is demonstrated. The transmitter consists of a sampled-grating DBR (SGDBR) laser and a series-push-pull Mach-Zehnder modulator. The pre-amplified receiver is composed of a flared semiconductor optical amplifier and a quantum well *pin* photodetector. Integrated resistors and capacitors are used to minimize microwave losses and remove the need for external bias tees. The design, fabrication and operation of this photonic integrated circuit is presented. Small signal response measurements show a device bandwidth in excess of 20 GHz. Operation at 40 Gbps with NRZ data shows less than a 2.5-dB power penalty across the 32 nm laser tuning range with no additional power penalty for conversion to the input wavelength.

Index Terms— tunable lasers, optical modulation, photonic integrated circuits (PICs), Mach-Zehnder modulator, semiconductor optical amplifier (SOA), sampled-grating DBR laser (SGDBR), offset quantum wells, wavelength converter.

I. INTRODUCTION

WAVELENGTH conversion will be an important part of the next generation of optical networks, allowing for dynamic wavelength management and enabling all-optical routers. These characteristics reduce wavelength blocking, where signal contention is an issue allowing the network to operate with lower latency and at bandwidths closer to capacity. Devices demonstrating bit-rate transparency, small form factors and low power consumption will best meet the demands of these networks. [1]

Monolithic approaches to wavelength conversion are particularly attractive due to their low packaging costs and increased scalability. High functionality photonic integrated circuits (PICs) have been achieved using straightforward integration platforms requiring only a single blanket regrowth and simple fabrication. These PICs remove the need for optical fiber coupling between individual components, which simplifies packaging and reduces power consumption. The small footprint of PICs make device arrays realizable.

One of the most extensively studied approaches to wavelength conversion is the use of semiconductor optical amplifiers (SOAs). These devices use cross gain modulation
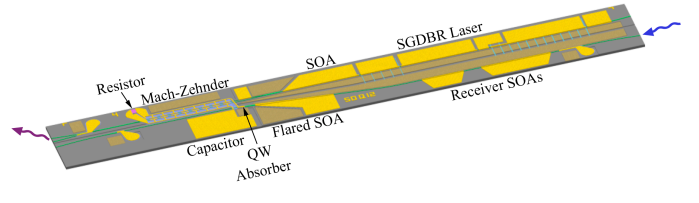
Fig. 1. Diagram of the SAM Mach-Zehnder wavelength converter

(XGM) or cross phase modulation (XPM) in a saturated SOA to convert the input signal to a new wavelength [2]. Filterless operation has been reported for SOA-based wavelength converters at 10 Gbps using Sagnac interferometers [3] and advanced Mach-Zehnder interferometers [4]. The bandwidth of SOA-based wavelength converters is inherently limited by carrier lifetime effects; however, there has been efforts using delayed interference techniques for return-to-zero data formats. Monolithically integrated devices including an on-chip laser and implementing delayed interferometers have been successfully reported at bit rates of 40 Gbps with return-to-zero data formats [5], [6].

Recently there has been success with the separate absorption and modulation (SAM) approach to wavelength conversion. In this method, a transmitter and receiver are monolithically integrated on a single chip. The photodiode is directly connected to the modulator allowing the photocurrent from an absorbed input signal to directly drive an optical electro-absorption modulator (EAM) [7]. Since the photodiode produces enough photocurrent to drive the optical modulator there is no need for any electrical amplification. Due to the spatial separation of the receiver and transmitter waveguides, SAM wavelength converters have no optical filtering requirements and are capable of conversion to the input wavelength. These devices also have the advantage of lower power consumption and smaller footprints than comparable SOA-based devices. Devices utilizing an external light source have demonstrated bit rates up to 500 Gbps [8]. Monolithic devices with regenerative capabilities at 10 Gbps have also been achieved [9]. It has also been shown that the integration of resistors and capacitors simplify the device operation by removing the need for external biasing and high-speed probes [7].

The work in this paper utilizes the SAM approach to wavelength conversion with Mach-Zehnder modulators (MZMs), instead of EAMs. Optical gates utilizing integrated photodetectors and MZMs with gate opening times as short as 5 ps

have been reported [10]. The use of MZMs are attractive for their ability to achieve zero or slightly negative chirp and high extinction ratios. Widely-tunable series-push-pull Mach-Zehnder modulator transmitters have demonstrated efficient operation at 40 Gbps [11] and negative chirp making them an important building block in this work. A widely tunable sampled-grating DBR (SGDBR) laser is used as the integrated light source allowing for tuning across 32 nm. The receiver is composed of a high saturation power SOA and an efficient quantum well photodetector. Wavelength conversion at 40 Gbps is achieved by taking advantage of the bandwidth benefits of traveling-wave device design. Microwave losses associated with high-speed probes and external bias tees are minimized by using a bias scheme requiring only DC probes and integrating a bypass capacitor and load resistor on-chip. Similar devices demonstrating error-free operation at 10 Gbps have been previously reported [12].

This paper is organized as follows; the Mach-Zehnder SAM wavelength converter is introduced in Section I. In Section II the material platform and fabrication of the device is discussed. Sections III and IV cover the design and performance of the transmitter and receiver sections respectively. Finally, Section V presents the biasing and operation of the fully integrated wavelength converter at 40 Gbps with an non-return-to-zero (NRZ) data stream. This is followed by a conclusion and summary of work.

II. INTEGRATION PLATFORM AND FABRICATION

The epitaxial material structure is grown by MOCVD on a semi-insulating substrate to allow for isolation between the transmitter and receiver ridges, as well as to reduce the capacitance of high speed pads. The wavelength converter's dual quantum well (DQW) integration platform is comprised of two sets of quantum wells (Fig. 2) [13]. A set of offset quantum wells (λ_{PL} = 1550 nm) are used in the gain section of the SGDBR and the SOAs. These wells are also reverse biased for use in the absorbing region. A separate set of seven quantum wells (λ_{PL} = 1465 nm) are centered in the 1.2-Q InGaAsP waveguide and aid the modulator efficiency by the utilization of the quantum confined Stark effect [14]. These centered wells are present throughout the device and therefore must be detuned from the operating wavelength to maintain low optical passive loss. An additional benefit of the centered quantum wells is the lower waveguide doping needed compared to bulk modulator regions. This means lower biases are necessary to fully deplete the waveguide, as well as more of the waveguide depleting thus reducing the ridge capacitance.

Initially, the offset quantum wells are removed with a wet etch from all passive areas (everywhere but the laser gain sections, the SOAs and the absorber), this is followed by dry etching of the holographically defined gratings in the grating burst regions. At this point, the single blanket regrowth of the InP cladding and InGaAs p-contact layer is performed. Following the regrowth, the ridges are are defined using a dry etch and a wet cleanup etch to insure smooth sidewalls. The device junction capacitance is reduced by etching into
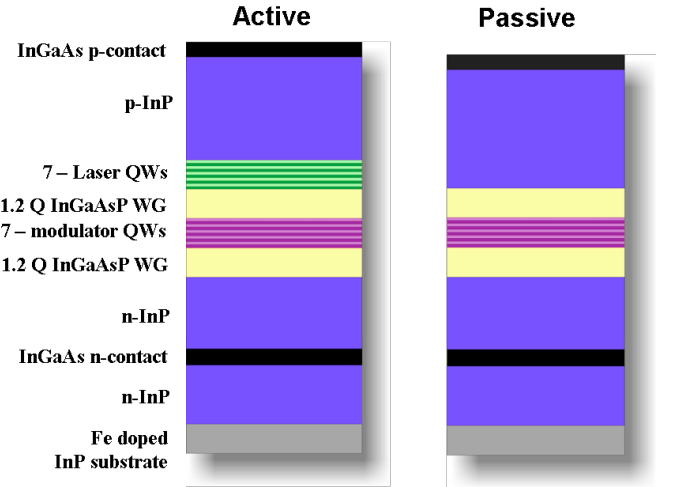

Fig. 2. Material structure of device. Epitaxial structure in the active regions is shown on the left and the passive regions is shown on the right.

the top 1000 $\mathring{A}$ of the waveguide, which became p-doped due to diffusion during the regrowth. The n-InGaAs contact layer is then exposed and the Ni/AuGe/Ni/Au n-contacts are deposited. The receiver and transmitter ridges are isolated by etching a 100 μm wide strip down to the Fe-doped substrate between the two ridges, at this time the semiconductor resistor is also isolated from the rest of the n-contact layer. Photo-bis-benzocyclobutene (BCB) deposited under the high speed pads reduces the device capacitance. The p-contacts are evaporated following BCB deposition and exposure of the ridge tops. A proton implant was used to electrically isolate the pads and to reduce optical losses.

The devices were then thinned, cleaved and a multi-layer antireflection (AR) coating was applied to the facets. In addition to the AR coating, curved and flared ridges were used to reduce facet reflections. The devices were mounted on aluminum nitride carriers for testing and the contacts were wirebonded to the carrier. All biases were applied with a DC probe card. The fabricated wavelength converter has a footprint of 3.3 mm × 0.46 mm.

III. TRANSMITTER

The five section widely tunable SGDBR laser used for the integrated light source consists of: a rear absorber, rear mirror, phase section, gain section and front mirror. These lasers are capable of achieving a quasi-continuous tuning range greater than 40 nm. Coarse tuning is achieved with a vernier based tuning mechanism controlled through current injection into the front and rear mirrors, while a phase sections allows for finer wavelength adjustment [15] [16]. A 500 μm long SOA follows the SGDBR allowing for power adjustments without effecting the lasing wavelength and blocking of the laser signal during wavelength tuning.

The Mach-Zehnder interferometer is composed of a 1×2 multimode interferometer (MMI) to split the light from the SGDBR and a 2×2 MMI to combine the light at the output. A forward-biased phase electrode within the Mach-Zehnder interferometer is used to insure the interferometer is biased
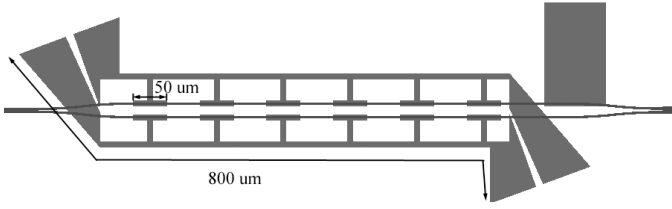
Fig. 3. Diagram of the test modulator transmission lines.

for maximum extinction ratios. The Mach-Zehnder modulator is operated in a series-push-pull fashion with the microwave signal from the photodiode applied across the tops of the two modulator arms. This configuration puts the two arms of the Mach-Zehnder in series along the microwave signal path. Therefore, the capacitance associated with the diodes is in series, effectively halving the device's capacitance. The reduction in device capacitance translates into higher bandwidths [17], [18]. Additionally, similar transmitters with series push-pull Mach-Zehnder modulators have been shown to produce output signals with negative chirp, which is important to maximize transmission distances [11]. It is expected these chirp characteristics will translate to the wavelength converted signal. Semiconductor resistors are integrated for on-chip terminations and to minimize the microwave loss.

The series-push-pull Mach-Zehnder modulator has been designed as a traveling wave structure with a characteristic impedance matched to 50 Ω. In order to reduce the transmission line capacitance thus increasing the transmission line characteristic impedance, the ridge width is reduced from 3 μm in the laser and SOA regions to 2 μm within the modulators. Additionally, the coplanar stripline (CPS) is capacitively loaded with periodic 50 μm long T-structures contacting the ridge. This configuration distributes the capacitance and increases CPS gap, which increases the characteristic impedance of the device. Unloaded, the transmission line impedance is 125 Ω. The Mach-Zehnder ridges add significant capacitance to the transmission line thus reducing the characteristic impedance to 50 Ω. Using s-parameter measurements as described in [19], the CPS transmission line parameters were extracted. All transmission lines measured were 800 μm long; however the number of T-structures was varied to change the amount of loading (Fig.3). The characteristic impedances for devices of lengths 300 μm (6 T-structures), 400 μm (8 T-structures) and 500 μm (10 T-structures) and loading of 38%, 50% and 63% respectively are shown in Fig. 4. The characteristic impedances for identical transmission line structures without loading are also shown in Fig. 4. The index of the transmission lines was also extracted yielding an index of 6, which although mismatched from the optical group index of 4 does not have a significant impact on the device bandwidth.

The wavelength converter utilizes a 300 μm long Mach-Zehnder modulator with six 50 μm long T-structures. Transmitter bandwidth measurements for a 300 μm long Mach-Zehnder modulator for co-propagating and counter-propagating electrical and optical waves were taken to con-
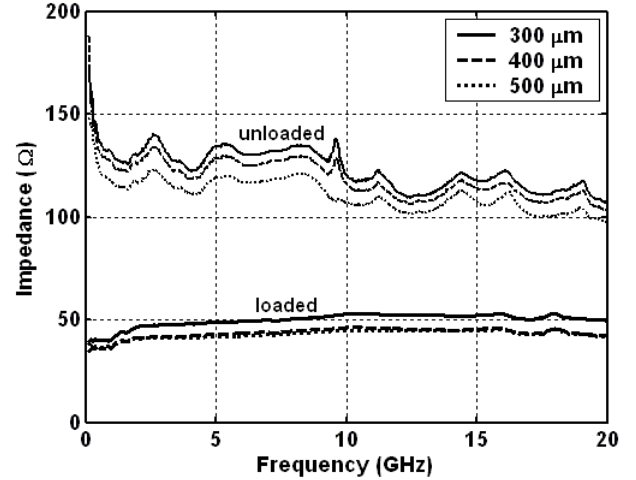

Fig. 4. Characteristic impedance of capacitively loaded transmission lines used in Mach-Zehnder modulator for unloaded lines and the loaded lines including the MZM ridge (V_{MZ1} = V_{MZ2} = -2 V).
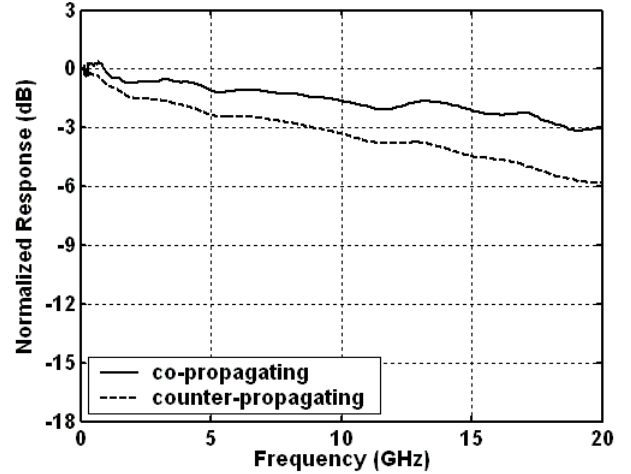

Fig. 5. Traveling wave bandwidth for 300 μm long Mach-Zehnder (V_{MZ1} = V_{MZ2} = -2 V and R_{load} = 50 Ω).

firm the traveling wave operation of the modulator (Fig. 5). These measurements show an 10 GHz improvement with co-propagation when the termination is matched to the transmission line impedance verifying the traveling wave operation of the device.

IV. RECEIVER

The receiver ridge is composed of linearly flared SOA and a 35 μm long taped quantum well photodetector [20]. The receiver section must generate enough photocurrent to drive the modulator while avoiding saturation effects. Quantum well detectors are quite attractive for their ease of integration with gain regions and their high absorption coefficient [21]. Saturating the photodetector will cause field screening problems due to trapped carriers thus reducing the device bandwidth. While the deep offset quantum wells are advantageous for providing carrier confinement in the gain regions of the wavelength converter, these same wells allow for poor carrier escape
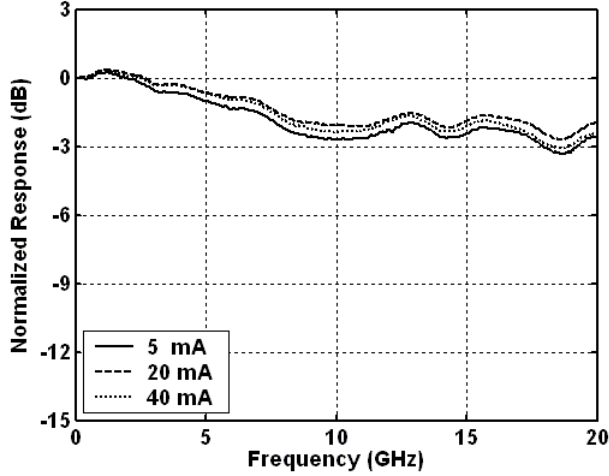
4

Fig. 6. Small signal measurements for a 50 μm long quantum well photodiode tapered from 9 μm to 2 μm (V_{PD} = -4 V, R_{load} = 25 Ω and P_{in} was varied).

Fig. 7. Simulation of the effects of ridge width and current density on output saturation power.

causing field screening which is detrimental when used as absorbing region. This is why it is necessary to provide a significant reverse bias (-4 V to -6 V) on the detectors to prevent saturation. Additionally, the detectors start off quite wide in the front end (9 μm) and taper off to 2 μm as more power is absorbed. This design allows for lower photocurrent densities at the front of the device, while still keeping area and capacitance to a minimum. The saturation characteristics of a 50 μm long photodetector have been measured by comparing the small signal response for various input photocurrents (Fig. 6), and no saturation effects have been observed for photocurrents up to 40 mA which is sufficient to drive the modulator. The small signal response measurements for this photodetector terminated in 25 Ω shows a bandwidth of 20 GHz.

The carrier density within an SOA will vary with significant input powers. The response time associated with a saturated SOA will induce pattern effects significantly degrading the converted signal. The saturation power of an SOA is governed by Equation 1 which shows the saturation power of the SOA can be increased by reducing any of the following parameters: carrier lifetime (τ), active region power density ($\Gamma_{xy}/(wd)$) or differential gain (a).

$$ G = G_o exp\left[-\frac{G-1}{G}\frac{P_o}{P_s}\right], P_s = \frac{wdh\nu}{a\Gamma_{xy}\tau} \tag{1} $$

The most straightforward way of increasing the saturation power is through the carrier lifetime which is inversely dependent on current density. Therefore, it is beneficial to operate the SOAs at the highest currents possible without the gain rolling over from heating. Further enhancements in the saturation power can be achieved by altering the geometry of the SOA to reduce the active region power density. In this work, the power density has been reduced by laterally flaring the SOA to provide a significant improvement in the device saturation power [20]. However, careful calculation of the flare length
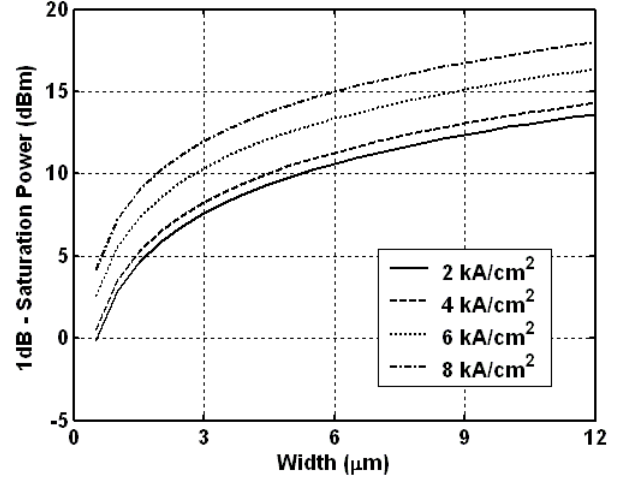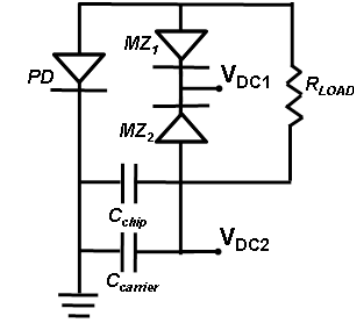

Fig. 8. Schematic of wavelength converter biasing.

and widths are necessary as wider SOAs will require more current adding to device power consumption and heating. Ideally the SOA will flare at the same rate as device gain staying just below saturation the whole way. These effects have been modeled and the results are shown in Fig. 7 [22].

The amplifiers in the wavelength converter were designed based upon the modeling. A 3 μm wide and 500 μm long straight SOA was implemented to boost the initial input power. This is followed by a 550 μm long SOA flared laterally from 3 μm to 12 μm wide to achieve high saturation powers. These amplifiers were coupled with 35 μm long tapered quantum well photodiodes. These receivers are polarization dependent due to the compressive strain in the quantum wells; therefore the input signal polarization was adjusted to TE to allow for maximum gain during all measurements. This dependence is typical of devices implementing strained quantum wells and could be eliminated through the redesign of the SOA and photodetector quantum wells [23].

V. Wavelength Converter

A. Biasing

It is beneficial to design a biasing scheme that allows for most of the electrical passive components to be integrated
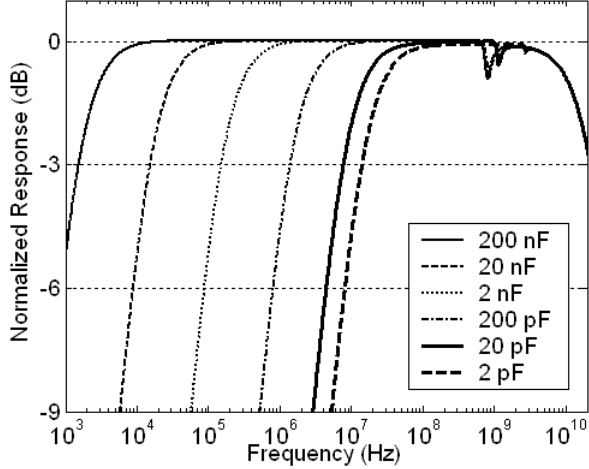
Fig. 9. Simulated effect of capacitor value on the low frequency cutoff value of the wavelength converter. The dip seen at 1 GHz is due to a LC resonance between the on-chip capacitor and the wirebonds to the on-carrier capacitor.

Fig. 10. Small signal response of wavelength converter. (R_{load} = 25 Ω; V_{DC2} = -5 V and varying values of V_{DC2}-V_{DC1}.)

onto the monolithic chip for the minimization of microwave losses, ease of testing and scalability of devices into arrays. The integration of resistors and capacitors insures that external bias tees are not needed for operation. The result of these efforts is the biasing scheme shown in Fig. 8. This biasing scheme allows direct bias control of one arm of the MZM. The other MZM arm and the photodiode are biased through the resistor; therefore, their exact bias point will vary based on the DC photocurrent level.

The on-chip termination resistor was fabricated from the InGaAs n-contact layer of the epitaxial material. In order to achieve the desired resistance value it is important to obtain an accurate measurement of the n-InGaAs sheet resistance. The sheet resistance was extracted using circular transfer length measurements (TLMs) [24] and the resistor dimensions were designed accordingly. This allowed the resulting resistors to be within 94 % of the desired value. The fabrication of these resistors require the material surrounding the resistor to be etched to the semi-insulating substrate thus providing proper electrical isolation from the rest of the device. The power handling capabilities of the resistor are quite good, as over 6 V can be applied across it without damage. Therefore, the resistors should not fail within the typical operating conditions of the wavelength converters.

An on-chip capacitor was used as a RF bypass capacitor for biasing. This parallel plate capacitor was formed from the InGaAs n-contact layer and the p-metal with 3000 $\mathring{A}$ of SiN$_x$ as the dielectric. The resulting capacitor has an area of 0.111 mm^2 and a capacitance of 19 pF. Since this on-chip capacitor is too small to provide a path for the signals low frequency components, an additional 220 nF on-carrier capacitor has been wirebonded in parallel with the integrated capacitor. The effect of the capacitor size on the low frequency cutoff of the wavelength converter can be seen in Fig. 9. Additionally, a small resistor (2 Ω) is used in series with the carrier capacitor to dampen any LC resonances caused by the inductance of the wirebonds.

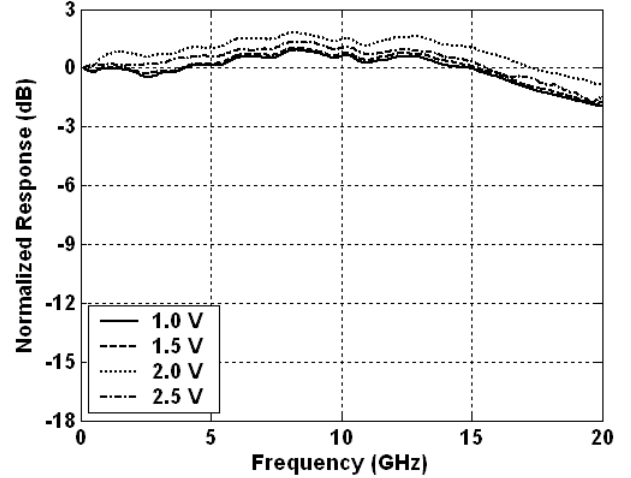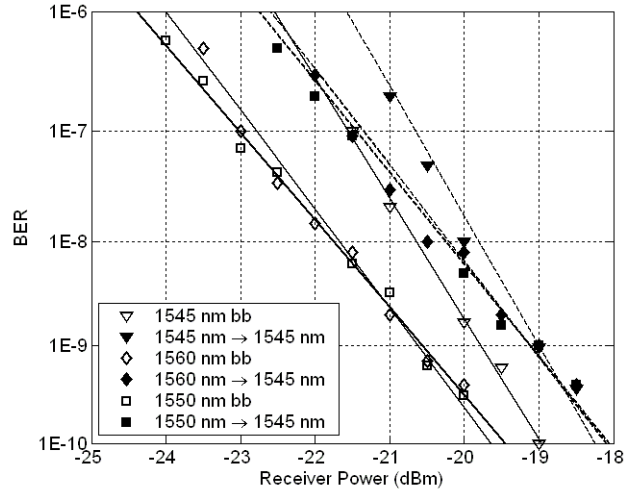Fig. 11. BER measurements for conversion at 40 Gbps for varying input wavelengths to an output wavelength of 1545 nm. Back to back measurements are plotted with solid lines and converted measurements are plotted with dashed lines. (P_{in} = 0.4 mW; I_{gain} = 100 mA; I_{T_xSOA} = 120 mA; I_{R_xSOA1} = 185 mA; I_{R_xSOA2} = 250 mA, V_{DC2}-V_{DC1}= -2 V and V_{DC2} = -5.6 V)

B. Experiments

The bandwidth of the device was measured using a HP3705A network analyzer. The wavelength converter demonstrated greater than 20 GHz bandwidth as shown in Fig. 10. The slight bandwidth enhancement seen at 10 GHz is due to the impedance mismatch between the 50 Ω transmission line of the Mach-Zehnder modulator and the 25 Ω integrated termination resistor. The improvement in bandwidth with reverse bias is due to a capacitance reduction from an increase in the depletion region of the device.

Bit error rate (BER) measurements with a NRZ 2^7-1 pseudorandom bit stream were taken with a 40 Gbps SHF bit-error-rate-tester (BERT). The word length was limited by the setup noise floor. The output of the BERT was amplified
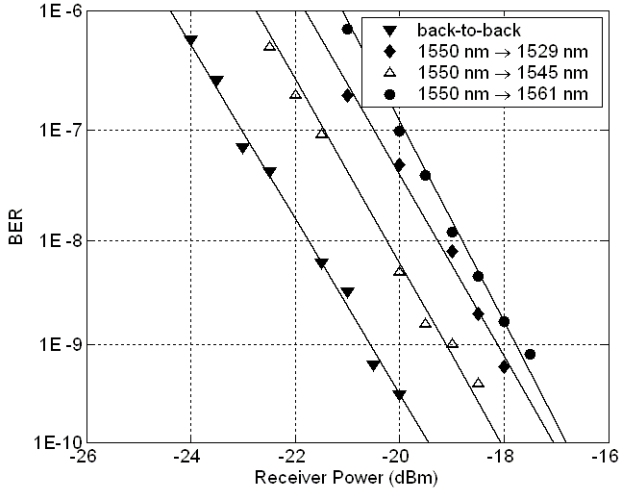
Fig. 12. 40 Gbps BER measurement for conversion from an input wavelength of 1550 nm to varying output wavelengths. (P_{in} = 0.4 mW; I_{gain} = 130 mA; $I_{T_x SOA}$ = 110 mA; $I_{R_x SOA1}$ = 185 mA; $I_{R_x SOA2}$ = 250 mA; V_{DC2}-V_{DC1}=-2 V and V_{DC2} = -5.6 V)
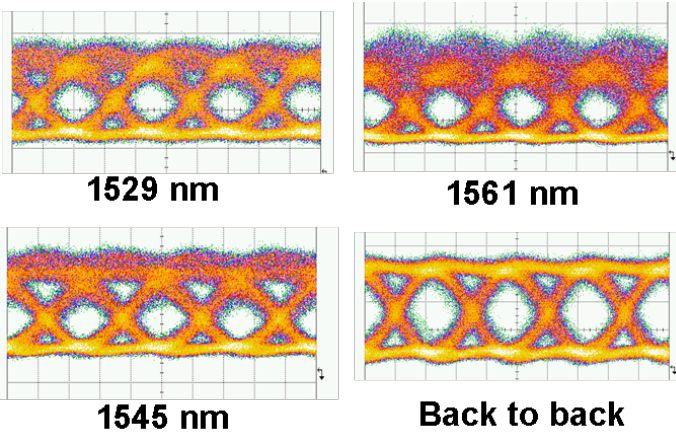

Fig. 13. 40 Gbps eye diagrams for conversion from 1550 nm to varying output wavelengths across the SGDBR tuning range.

by a high power eribum doped amplifier (EDFA), followed by a polarization controller before being coupled into the wavelength converter using a conically tipped lensed fiber. The output of the wavelength converter was coupled into a conically tipped lensed fiber and connected directly to the commercial pre-amplified optical receiver.

In order to achieve the bandwidth necessary for error-free operation at 40 Gbps, a high-speed ground-signal probe terminated in 50 Ω was placed in parallel with the integrated 25 Ω termination resistor. This configuration makes the effective termination 17 Ω. In future device fabrication runs, the resistor can be designed for a smaller value and no high-speed probes would be necessary. The input power was 0.4 mW, which generated 28 mA of photocurrent in the photodetector. These power levels allow the SOA to be operated below the output saturation power. All measurements were taken at a temperature of 19° C. The DC bias points on the MZM and photodiode were -2 V and -5.6 V respectively.

Error free operation was achieved for conversion between varying input wavelengths and an output wavelength of 1545 nm. The BER measurements showed power penalties less than 2 dB (Fig. 11). One of the advantages of the SAM wavelength converters is the ability to convert to the input wavelength and the BER measurements confirm this with no additional power penalty for input wavelength conversion. The change in slope of the back-to-back and converted BER measurements for an input power of 1545 nm is due to the wavelength dependance of the commercial transmitter used in the test setup. Bit-error-rate measurements were also taken for conversion from 1550 nm to wavelengths across the SGDBR tuning range (1528 nm-1561 nm) resulting in power penalties less than 2.5 dB (Fig. 12). The open eye diagrams for this conversion experiment are seen in Fig. 13. The increased power penalty for conversion to 1561 nm is due to the decreased efficiency of the modulator at longer wavelengths. The coupling loss between the chip and fiber were approximated to be 3 dB for both the input and output facets. The wavelength converter was operated with an input power of -4 dBm and output powers of -7 dBm; therefore, the device facet-to-facet conversion efficiency was -3 dB.

VI. CONCLUSION

A monolithic separate absorption and moduation region (SAM) wavelength converter has been fabricated with an integrated resistor and capacitor. This device presents a realizable solution for wavelength conversion with a small footprint and low-power dissipation. The transmitter ridge consists of a widely tunable SGDBR and a traveling-wave series-push-pull Mach-Zehnder modulator. The receiver ridge utilizes a high-saturation power flared SOA and a tapered quantum well absorber. This device requires no external bias tees due to the integration of a parallel plate capacitor and semiconductor resistor. The spatial separation of the input and output wavelengths allows for no optical filtering requirement.

The wavelength converter's small signal response measurements showed a bandwidth in excess of 20 GHz. This Mach-Zehnder SAM wavelength converter is the first monolithic wavelength converter reported to operate at 40 Gbps using NRZ data. Characterization at 40 Gbps demonstrated power penalties of less than 2.5 dB across the laser tuning range of 32 nm. Additionally, there was no additional power penalty observed for conversion to the input wavelength.

REFERENCES

[1] M. Borella, J. Jue, D. Banerjee, B. Ramamurthy, and B. Mukherjee, "Optical components for WDM lightwave networks," *Proceedings of the IEEE*, vol. 85, no. 8, pp. 1274–1307, 1997.

[2] T. Hatta, T. Miyahara, Y. Miyazaki, K. Takagi, K. Matsumoto, T. Aoyagi, K. Motoshima, K. Mishina, A. Maruta, and K. Kitayama, "Polarization-Insensitive Monolithic 40-Gbps SOA MZI Wavelength Converter With Narrow Active Waveguides," *IEEE Journal of Selected Topics in Quantum Electronics*, vol. 13, no. 1, pp. 32–39, 2007.

[3] Y. Shibata, N. Kikuchi, S. Oku, I. Ito, H. Okamoto, Y. Kawaguchi, Y. Kondo, Y. Suzuki, and Y. Tohmori, "Filter-free all-optical wavelength conversion using sagnac interferometer integrated with parallel-amplifier structure (sipas)," *Electronics Letters*, vol. 38, no. 21, pp. 1273–1275, 2002.

[4] D. Wolfson, T. Fjelde, A. Kloch, C. Janz, F. Poingt, F. Pommereau, I. Guillemot, F. Gaborit, and M. Renaud, "Detailed experimental investigation of all-active dual-order mode Mach-Zehnder wavelength converter," *Electronics Letters*, vol. 36, no. 15, pp. 1296–1297, 2000.

[5] V. Lal, M. L. Masanovic, J. A. Summers, G. Fish, and D. J. Blumenthal, "Monolithic Wavelength Converters for High-Speed Packet-Switched Optical Networks," *Selected Topics in Quantum Electronics, IEEE Journal of*, vol. 13, no. 1, pp. 49–57, 2007.

[6] P. Bernasconi, L. Zhang, W. Yang, N. Sauer, L. L. Buhl, J. H. Sinsky, I. Kang, S. Chandrasekhar, and D. T. Neilson, "Monolithically Integrated 40-Gb/s Switchable Wavelength Converter," *Journal of Lightwave Technology*, vol. 24, no. 1, pp. 71–76, January 2006.

[7] M. Dummer, M. Sysak, J. Raring, A. Tauke-Pedretti, and L. Coldren, "Widely Tunable Single-Chip Transceiver for 10 Gb/s Wavelength Conversion," in *Device Research Conference (DRC)*, no. II.A-3, University Park, PA, June 2006.

[8] S. Kodama, T. Yoshimatsu, and H. Ito, "500 Gbit/s optical gate monolithically integrating photodiode and electroabsorption modulator," *Electronics Letters*, vol. 40, no. 9, pp. 555–556, 2004.

[9] M. Sysak, J. Raring, J. Barton, H. Poulsen, D. Blumenthal, and L. Coldren, "Extinction ratio regeneration, signal re-amplification (2R), and broadband wavelength switching using a monolithically integrated photocurrent driven wavelength converter," *Optics Express*, vol. 14, no. 23, pp. 11 348–11 353, November 2006.

[10] T. Yoshimatsu, S. Kodama, and H. Ito, "InP-based ultrafast optical gate monolithically integrating uni-travelling-carrier photodiode and Mach-Zehnder modulator," *Electronics Letters*, vol. 41, no. 22, pp. 1243–1244, 2005.

[11] A. Tauke-Pedretti, M. Sysak, J. Barton, J. Raring, L. Johansson, and L. Coldren, "40-Gb/s Series-Push-Pull Mach-Zehnder Transmitter on a Dual-Quantum-Well Integration Platform," *IEEE Photonics Technology Letters*, vol. 18, no. 18, pp. 1922–1924, September 15 2006.

[12] A. Tauke-Pedretti, M. Dummer, J. S. Barton, M. N. Sysak, J. W. Raring, J. Klamkin, and L. A. Coldren, "Widely tunable 10 Gbit/s separate absorption and modulation Mach-Zehnder wavelength converter," *Electronics Letters*, vol. 43, no. 10, pp. 584–585, 2007.

[13] M. Sysak, J. Raring, J. Barton, M. Dummer, D. Blumenthal, and L. Coldren, "A single regrowth integration platform for photonic circuits incorporating tunable SGDBR lasers and quantum-well EAMs," *IEEE Photonics Technology Letters*, vol. 18, no. 15, pp. 1630–1632, August 2006.

[14] J. S. Weiner, D. A. B. Miller, and D. S. Chemla, "Quadratic electro-optic effect due to the quantum-confined Stark effect in quantum wells," *Applied Physics Letters*, vol. 50, no. 13, pp. 842–844, 1987.

[15] L. C. V. Jayaraman, Z.M. Chuang, "Theory, design, and performance of extended tuning range semiconductor lasers with sampled gratings," *IEEE Journal of Quantum Electronics*, vol. 29, no. 6, pp. 1824–1834, June 1993.

[16] L. A. Coldren, "Monolithic tunable diode lasers," *Selected Topics in Quantum Electronics, IEEE Journal of*, vol. 6, no. 6, pp. 988–999, 2000.

[17] J. S. Barton, M. L. Masanovic, A. Tauke-Pedretti, E. J. Skogen, and L. A. Coldren, "Monolithically-integrated 40 Gbit/s widely-tunable transmitter using series push-pull Mach-Zehnder modulator SOA and Sampled-Grating DBR laser," in *Optical Fiber Communication Conference and Exposition and The National Fiber Optic Engineers Conference*, Anaheim, CA USA, March 2005, paper OTuM3.

[18] R. G. Walker, "High-speed III-V semiconductor intensity modulators," *IEEE J. Quantum Electron.*, vol. 27, pp. 654–667, Mar. 1991.

[19] R. Spickermann and N. Dagli, "Experimental analysis of millimeter wave coplanar waveguide slow wave structures on GaAs," *IEEE Transactions on Microwave Theory and Techniques*, vol. 42, no. 10, pp. 1918–1924, October 1994.

[20] A. Tauke-Pedretti, M. Dummer, J. S. Barton, M. N. Sysak, J. W. Raring, and L. A. Coldren, "High Saturation Power and High Gain Integrated Photoreceivers," *IEEE Photon. Technol. Lett.*, vol. 17, no. 10, pp. 2167–2169, Oct. 2005.

[21] B. Mason, S. Chandrasekhar, A. Ougazzaden, C. Lentz, J. Geary, L. Buhl, L. Peticolas, K. Glogovsky, J. Freund, L. Reynolds, G. Przybylek, F. Walters, A. Sirenko, J. Boardman, T. Kercher, M. Rader, J. Grenko, D. Monroe, and L. Ketelsen, "Photonic integrated receiver for 40 Gbit/s transmission," *Electronic Letters*, vol. 38, no. 20, pp. 1196–10 097, September 2002.

[22] V. Lal, W. Donat, A. T. Pedretti, L. Coldren, D. Blumenthal, and J. Piprek, "Broadband Rate-Equation Model including Many-Body Gain for WDM Traveling-Wave SOAs," in *5th International Conference Numerical Simulation of Optoelectronic Devices*, Berlin, Germany, September 2005, pp. 125–126.

[23] D. Wake, S. Judge, T. Spooner, M. Harlow, W. Duncan, I. Henning, and M. O'Mahony, "Monolithic integration of 1.5 um optical preamplifier and PIN photodetector with a gain of 20 dB and a bandwidth of 35 GHz," *Electronic Letters*, vol. 26, no. 15, pp. 1166–1168, July 19 1990.

[24] J. Klootwijk and C. Timmering, "Merits and Limitations of Circular TLM structures for contact resistance determination for novel III-V HBTs," in *Proceeding of IEEE 2004 Conference on Microelectronic Test Structures*, vol. 17, March 2004, pp. 247–252.

Anna Tauke-Pedretti received the B.S. degree in Physics and Electrical Engineering from the University of Iowa, Iowa City, in 2001, and the M.S. and Ph.D. degrees in Electrical and Computer Engineering from the University of California, Santa Barbara, in 2002 and 2007 respectively. Her current research interests focus on InP-based photonic integrated circuits for high-speed wavelength conversion. She has also developed monolithic high-speed transmitters and high-saturation power pre-amplified receivers.

Matthew M. Dummer received the B.S. degree in Electrical Engineering from the University of Minnesota 2002, and the M.S. from the University of California, Santa Barbara in 2004. He is currently at UCSB pursuing the Ph.D. His research focuses on high functionality photonic integrated circuits for wavelength conversion. He also specializes in the fabrication of high power semiconductor optical amplifiers and photodiodes, as well as traveling wave circuit design for electroabsorption modulators.

Matthew N. Sysak received his B.S. degree in Chemical Engineering from the Pennsylvania State University in 1998, and his M.S. and Ph.D. degrees from the University of California Santa Barbara in 2002 and 2005, respectively. His PhD thesis focused on material design as well as device design, fabrication, and testing of monolithically integrated, widely tunable, optoelectronic wavelength converters and signal regenerators. Following his PhD, Dr. Sysak joined Prof. John Bowers' research group as a Post-Doctoral Scholar where he worked on novel photonic circuit design and fabrication for analog, phase modulated links. In 2007 he joined Intel Corporation in Santa Clara, CA, where he is working on silicon photonic integrated circuits. Dr. Sysak has authored and coauthored over 50 conference and journal papers, has been an invited speaker at several technical meetings, and is a member of OSA, IEEE, and SPIE.

Jonathon S. Barton was born in Sacramento, CA, in 1975. He earned the B.S. degree in Electrical Engineering and Material Science Engineering, at the University of California, Davis in 1998. He was an Intel fellow in 2004 and completed the Ph.D. degree in Electronic Materials at the University of California, Santa Barbara in 2004. At the University of California, Santa Barbara, he pioneered work on C-band 40 Gbps tunable monolithically integrated Mach-Zehnder transmitters. Furthermore, he has coauthored over seventy papers, invited and contributed talks on tunable lasers and photonic integrated circuits, at various international conferences.

Jonathan Klamkin received the B.S. degree in Electrical and Computer Engineering from Cornell University in 2002, the M.S. degree in Electrical and Computer Engineering from the University of California, Santa Barbara (UCSB) in 2004, and is now working toward the Ph.D. degree in Materials at UCSB. His research interests include the design, growth, fabrication, and characterization of widely-tunable semiconductor lasers, photodetectors, optical intensity and phase modulators, and semiconductor optical amplifiers for InP based photonic integrated circuits. Currently his efforts are focused on novel coherent integrated receivers for highly linear fiber-optic links.

James W. Raring earned the B.S. degree from the materials engineering department at California Polytechnic State University, San Luis Obispo in 2001 and the Ph.D. in materials science from the University of California, Santa Barbara in 2006. His research focused on the design, growth, and fabrication of high-functionality wavelength-agile In-GaAsP based photonic integrated circuits (PIC). By coupling quantum well intermixing with MOCVD regrowth, he combined widely-tunable sampled grating DBR lasers, 40 Gb/s electroabsorption modulators, low-confinement high-saturation power semiconductor optical amplifiers, and 40 Gb/s uni-traveling carrier photodiodes to demonstrate the first single-chip 40 Gb/s optical transceiver. In 2006, James joined the RF/optoelectronic group at Sandia National Laboratories where he continues to work on leading edge PICs. He has authored or co-authored over 70 technical papers and is a member of IEEE LEOS, OSA and SPIE.

Larry A. Coldren received the Ph.D. degree in electrical engineering from Stanford University, Stanford, CA in 1972. After 13 years in the research area at Bell Laboratories, he joined the University of California, Santa Barbara (UCSB), in 1984, where he is now the Fred Kavli Professor of optoelectronics and sensors, and the Director of the Optoelectronics Technology Center. In 1990, he cofounded Optical Concepts, later acquired as Gore Photonics, to develop novel vertical cavity surface-emitting laser (VCSEL) technology and in 1998 he cofounded Agility Communications to develop widely tunable integrated transmitters. At Bell Laboratories, he initially worked on waveguided surface-acoustic wave signal processing devices and coupled-resonator filters. He later developed tunable coupled-cavity lasers using novel reactive-ion etching (RIE) technology that he created for the then new InP-based materials. At UCSB he continued work on multiple-section tunable lasers, inventing, in 1988, the widely tunable multi-element mirror concept. During the late 1980s, he also developed efficient vertical-cavity multiple-quantum-well modulators, which led to novel VCSEL designs that provided unparalleled levels of performance.

His current research interests include developing new photonic integrated circuit (PIC) and VCSEL technology, including the underlying materials growth and fabrication techniques, creation of vertical and in-plane GaN-based emitters, efficient all-epitaxial InP-based VCSELs, and a variety of PICs incorporating numerous optical elements for widely tunable integrated transmitters, receivers, and wavelength converters. He has authored or coauthored over 700 papers, five book chapters, one textbook, and is a holder of 36 patents. Prof. Coldren has presented dozens of invited and plenary talks at major conferences. He is a Fellow of the Optical Society of America and Institute of Electrical Engineers, and a member of the National Academy of Engineering. He was the recipient of the 2004 John Tyndall Award.